High Resolution Studies of the Lyman α Forest

David Peter Mar

A thesis
submitted for the degree of
Doctor of Philosophy
at the
University of Sydney

August, 1995
Revised: February, 1996

Abstract

This thesis presents a study of the Lyman α forest clouds along the sightlines to the high-redshift QSOs 1101−264 and 2348−147. A preliminary study is made of a detailed simulation of a QSO spectrum in order to characterise the biases present in the data reduction and analysis techniques. The information gained is used to aid the interpretation of several observational properties of the Lyman α clouds:

- The distribution of neutral hydrogen column densities.
- The evolution of cloud number density with redshift.
- The distribution of velocity dispersions in the absorbing gas.
- The spatial clustering of the clouds.

The metal line systems in the spectra of the QSOs are also described and a search is made for the presence of metals in Lyman α forest systems. Some observations on the shapes of the QSO Lyman α emission line profiles are made. A comparison between various QSO sightlines is performed to gauge the validity of extrapolating information from one sightline to large regions of high-redshift space.

Preface

> This is what it is to be human: to see the essential existential futility of all action, all striving—and to act, to strive... to reach forever beyond your grasp... to live forever or die trying... to perpetually ask the unanswerable questions, in the hope that the asking of them will somehow hasten the day when they will be answered.
>
> — Spider and Jeanne Robinson, *Stardance*.

Acknowledgements

It has been both an interesting and an entertaining few years working on this project. No mission of such magnitude, however, is completed alone. Therefore, the following crew members of this *Enterprise* must be acknowledged.

For the opportunity and the necessary guiding expertise I wish to thank my supervisor, Richard Hunstead, the Captain Jean-Luc Picard of the ongoing mission. Max Pettini, as first officer Commander William Riker, also gave me advice and instruction in many areas of this work, particularly in the practical training necessary to master the data reduction software I used and with valuable comments on manuscripts.

Every project must have an engineering crew. Acting as my Geordie La Forge, the staff at the Anglo-Australian Observatory and the Anglo-Australian Telescope have been encouraging and helpful. Jason Spyromilio and Sean Ryan assisted with technical help during observing sessions and taught me a great deal about using telescopes and other astronomical instruments. All the AAT night assistants performed invaluable jobs, and Gordon Shafer in particular must be thanked for arranging fine weather during several of my observing runs, and coping with my taste in observing music. The Australian Time Assignment Committee were generous in assigning observing time on the AAT to my project.

I spent four weeks working at Princeton University, and I thank Ed Jenkins and Jerry Ostriker, administrators of this prestigious Starfleet Academy, for making that stay possible. Ed also contributed a substantial component of the data for my study, putting a great deal of effort into creating the large and complex "Cloudy Night QSO" simulation on which to test my data reduction procedures, for which I am very grateful.

Geoff Bailey provided substantial assistance with computer programming tasks, especially by writing the X Window System user interface for the Xvoigt program which I developed, but also with other random debugging. Keith Lipman used Xvoigt extensively, providing helpful suggestions, and also helped me with several metal system line identifications in my data. Together, they made an excellent Lieutenant-Commander Data.

Brad Peterson of Ohio State University was friendly and helpful when I e-mailed him out of the blue to ask myriad questions about AGN emission line structure. Raylee Stathakis performed service observations of the QSO 2348−147 at low resolution, providing valuable data on this object redward of Lyman α emission. Danny Yee performed a remarkable job of proofreading this entire tome within the space of only a few days. Lieutenant Worf would have been proud to offer such ready assistance.

My office-mates for the past few years were very helpful and supportive, playing Guinan admirably. Jo Baker provided much useful knowledge about quasars in general, corroborative appreciation of classical music, and lots of excuses to buy chocolate. (If only she hadn't finished before me and gone home to England when I was assembling Chapter 1!) Ann Burgess was a fount of wisdom on radio properties and other aspects of general astronomy and all those fiddly bits of warp-field theory mathematics I forgot.

Counsellor Deanna Troi is responsible for the emotional well-being of her companions when all else fails. For their empathy, patience, and encouragement, I thank Amanda Lang, Ariane Hemming, Sue Byleveld, Lachlan Patrick, and Claire Garrity.

The following people all helped in various non-technical ways, playing Doctor Beverley Crusher to some of the coughs and colds along the way:
Lynn Alford, Stephanie Alford, Alfvaen (Aaron V. Humphrey), Elana Beach, Saskia Besier, Louis J. Bookbinder, Jay Brandt, Mary Branscombe, Johanna Colgrove, Kelly J. Cooper, Rachel Crawford, Faith Harvey, Mike Holmes, Janet Huss, Merrill Kaplan, Thomas J. Lee, Liralen Li (Phyllis Rostykus), Michelle Morgan, John Mark Ockerbloom, Mary Mark Ockerbloom, Abner Mintz, Elena O'Malley, John Palmer, Heather Patrick, Meredith Rosser, Barbara Trumpinski (the purple-haired, leather-skirted, studded-collared, whip-wielding, electro-cuty, Biker Punk Librarian Wench from Hell), Mike Wasson, Mike Whitaker.

For Michelle.

Statement of Originality

This thesis describes work carried out in the Department of Astrophysics at the University of Sydney between 1990 and 1995. Except where acknowledged otherwise, the work presented in this thesis is my own. The major contributions from other people are as follows:

- Professor Ed Jenkins produced the detailed simulation of a QSO spectrum, known as the Cloudy Night QSO spectrum, described and analysed in Chapters 2 and 3.
- Geoff Bailey did a substantial amount of computer programming for the Xvoigt software package which we developed to analyse absorption lines.
- Max Pettini and Richard Hunstead provided feedback and suggestions on all of the continuum fits and metal line identifications.

D. P. Mar
Sydney, Australia
August, 1995

Astronomical Units

For consistency with much of the published work in astronomy, the following non-SI units are used in this thesis:

- The angstrom (Å):

$$1\,\text{Å} = 10^{-10}\,\text{m}. \tag{0.1}$$

- The milliangstrom (mÅ):

$$1\,\text{mÅ} = 10^{-13}\,\text{m}. \tag{0.2}$$

- The centimetre (cm):

$$1\,\text{cm} = 10^{-2}\,\text{m}. \tag{0.3}$$

- The parsec (pc):

$$1\,\text{pc} \simeq 3.08 \times 10^{16}\,\text{m}. \tag{0.4}$$

- The kiloparsec (kpc):

$$1\,\text{kpc} \simeq 3.08 \times 10^{19}\,\text{m}. \tag{0.5}$$

- The megaparsec (Mpc):

$$1\,\text{Mpc} \simeq 3.08 \times 10^{22}\,\text{m}. \tag{0.6}$$

- The erg:

$$1\,\text{erg} = 10^{-7}\,\text{J}. \tag{0.7}$$

Contents

List of Tables

List of Figures

Chapter 1

Introduction

1.1 QSOs—Probes of Intergalactic Space

In 1963 the peculiar radio source 3C 273 was identified with a 12th magnitude stellar object which was discovered to possess an optical spectrum in which the atomic emission lines were shifted towards the red with a fractional wavelength increase, or *redshift*[1], of $z_{\rm em} = 0.16$ (Schmidt, 1963). Objects of higher redshift were known at the time but assuming the redshift was cosmological in origin[2], and therefore an indicator of great distance, implied that 3C 273 was much more luminous at optical wavelengths than any other known object.

3C 273 was designated a "quasi-stellar radio source" because it was a point source resembling a star at optical wavelengths. This name has since been contracted to "quasar". Other bright, point-like objects of even larger redshifts were rapidly discovered and it became clear that most were not strong radio sources. These were called "quasi-stellar objects", which later became "QSOs"[3].

When it was established beyond reasonable doubt that QSO redshifts were cosmological (see Weedman, 1976, for a review), it became obvious that QSOs provided one of the most powerful observational tools for studying the early universe. QSOs are the most distant observable objects and the most luminous, so a study of their spectra can provide information about physical conditions at an earlier time than most other observations.

The most distant known QSOs today, at redshifts $z \sim 5$, reveal glimpses of the universe at a time when it was less than 10% of its present age.

---

[1]The redshift z of a spectral feature is defined by the relation $(1 + z) = \lambda_{\rm obs}/\lambda_0$, where $\lambda_{\rm obs}$ is the observed wavelength and λ_0 is the rest wavelength.

[2]There are three possible causes of redshift: (1) Doppler shift, caused by a relative velocity difference between the radiation source and the observer. Doppler shift can be either redshift or its complement, blueshift. (2) Cosmological redshift, caused by the expansion of the universe between the time of emission and the time of reception. (3) Gravitational redshift, caused by the loss of photon energy as it passes through a gravitational field. Gravitational redshift is negligible except in extremely strong gravitational fields, such as in the immediate vicinity of black holes.

[3]The quasar/QSO nomenclature is often considered now to be interchangeable between radio-loud and radio-quiet objects, though this has not been the case in the past.

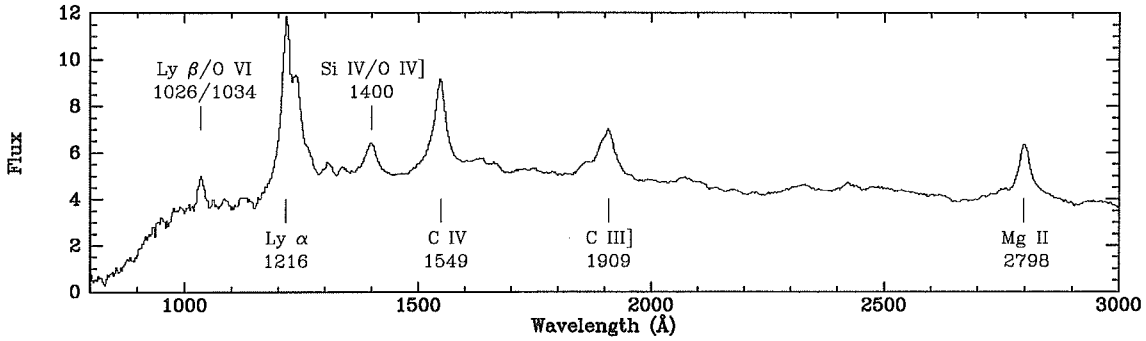

Figure 1.1 A composite spectrum of 718 QSOs, taken from Francis *et al.* (1991). The flux is plotted as $\lambda F(\lambda)$ in arbitrary units. Prominent emission lines are marked, with their wavelengths in angstroms (rounded to the nearest integer).

1.1.1 Optical QSO Spectra

Much of the information gathered from QSOs comes from spectral observations made at optical wavelengths. The high redshifts of QSOs mean that portions of the near ultraviolet spectrum are shifted into optical wavelengths. These wavelengths are rich in spectral lines of many elements, and it is through studying the emission lines that much of the knowledge about QSOs has been compiled (Weedman, 1986, pp164–187).

A composite QSO spectrum for rest wavelengths $800 < \lambda_0 < 3000$ Å, formed by summing the spectra of 718 QSOs in the rest frame (Francis *et al.*, 1991), is shown in Figure 1.1. The spectrum is at an intermediate spectral resolution of 4 Å full-width-at-half-maximum (FWHM). It clearly shows the broad permitted emission lines which are characteristic of QSOs. The broad emission lines typically have widths[4] $\gtrsim 10^4\,\mathrm{km\,s^{-1}}$.

The strongest QSO emission line is usually the resonance line of neutral hydrogen, H I λ1215[5], also known as Lyman α. The Lyman α line arises from the first transition in the Lyman series of hydrogen, when the electron moves from principal quantum number $n = 2$ to $n = 1$. The H I λ1025 (Lyman β, $n = 3$ to $n = 1$) line is also visible in Figure 1.1, as well as lines of Si IV/O IV][6], C IV, C III], and Mg II.

[4]Spectral line widths and spectral resolutions are often quoted in units of velocity. The velocity difference Δv associated with a wavelength difference of $\Delta\lambda$ is defined by $\Delta v = c\Delta\lambda/\lambda_0$, where c is the speed of light and λ_0 is the wavelength at which the width/resolution is being quoted.

[5]Throughout this thesis, spectral lines are referred to with the standard labelling, consisting of: The chemical symbol for the element, a Roman numeral indicating the ionisation state (I = neutral, II = singly ionised, III = doubly ionised, etc.), the Greek letter λ indicating wavelength, and the wavelength of the line in angstroms, truncated to a whole number (or one decimal place if needed to remove ambiguity).

[6]The single right bracket indicates a semi-forbidden transition.

1.2 QSO Absorption Lines—Historical Background

When observed at moderate spectral resolution ($\sim$ 75–150 km s^{-1}, or $\sim$ 1–2 Å at $\lambda = 4000$ Å), optical spectra of high-redshift ($z_{\rm em} \gtrsim 2$) QSOs are seen to contain an abundance of absorption lines, mostly concentrated blueward of the Lyman α emission line. The effect of this can be seen on the lower resolution composite spectrum shown in Figure 1.1, through the apparent drop in the continuum emission level on the blue side of the Lyman α emission peak. (In this case, the absorption lines are unresolved. A spectrum in which the lines are resolved is shown in Figure 1.2.)

Lynds first drew attention to this curious phenomenon in a talk given at IAU Symposium 44 in Uppsala, Sweden, in 1970 (later published as Lynds, 1972). Lynds (1971) suggested that most of the absorption lines blueward of Lyman α emission were caused by Lyman α absorption in numerous "clouds" of hydrogen at intermediate redshifts. This could explain naturally the asymmetric distribution of absorption around the emission redshift $z_{\rm em}$. An alternative hypothesis was that the absorption was in material physically associated with the QSO, possibly ejected along the line of sight at high velocities.

A small fraction of QSOs ($\sim$ 5–10%) do in fact show absorption features which are incontrovertibly intrinsic to the QSO. These are the broad absorption line (BAL) QSOs, defined by Weymann *et al.* (1981). BAL QSOs show extremely broad troughs of absorption, extending up to 20 000 km s^{-1} or more to the blue of the emission line peaks. Turnshek *et al.* (1980) demonstrated that the BAL features are almost certainly caused by absorption in gas outflowing from the central source.

Most of the absorption lines seen in non-BAL QSOs[7] are relatively narrow—unresolved at spectral resolutions of $\gtrsim 40$ km s^{-1} ($\gtrsim 0.5$ Å). Usually, some of these lines can be identified as arising from metal[8] absorption in well-defined systems of common redshift. These metal systems occur at absorption redshifts $z_{\rm abs} \leq z_{\rm em}$, where galactic haloes or discs happen to intercept the line of sight to the QSO. Typically there are several metal systems at different absorption redshifts in any QSO spectrum, but they account for only a small fraction of the absorption lines.

The numerous unidentified absorption features seen blueward of Lyman α emission were not fully understood for some years after their discovery by Lynds. It was not clear whether they represented absorption by material ejected from the QSO at high velocity along our line of sight or by material distributed cosmologically along the sightline. The theory that the mysterious lines were produced by intervening clouds of hydrogen received strong support when:

- Young *et al.* (1979) found a strong peak at the Lyman α/Lyman β ratio in a cross-correlation of the spectrum of the $z_{\rm em} = 3.280$ QSO PKS 2126−158,

[7]Hereafter in this thesis, for simplicity, the term "absorption lines" or similar terms will be taken to exclude the BAL systems, except where specifically noted otherwise.

[8]Following normal astronomical practice, the term "metal" is used to refer to all elements other than hydrogen and helium.

implying that $\gtrsim 90\%$ of the absorption lines blueward of Lyman α emission were due to Lyman α.

- Sargent *et al.* (1980, hereafter SYBT) presented statistical evidence from a homogeneous sample of five QSOs showing no correlations between any of the parameters: Absorption line numbers, line strength, redshift, and background object. These observations severely constrained any possible ejection theory, while they arose naturally in simple intervening cloud models.
- Oke and Korycansky (1982) pointed out that any Lyman α absorption caused by material ejected from a QSO would preferentially appear near the Lyman α emission line (most likely in the line wing). With the exception of the BAL systems in some QSOs, no systematic differences between absorption lines far from and near the emission peak was evident. Also, lines with black cores (in which the QSO light is fully absorbed) occurred in the emission wings (Lowrance *et al.*, 1972), requiring the absorber to cover the line-emitting region and implying a highly improbable velocity structure if the absorbing material was physically associated.

With the establishment of the intervening cloud hypothesis, it is possible to describe in general terms how the various features of an intermediate resolution QSO spectrum are formed. A typical spectrum, showing the absorption lines in the vicinity of Lyman α emission, and accompanying sketch showing the arrangement of material along the line of sight to the QSO are presented in Figure 1.2. The plethora of Lyman α absorption lines is called the *Lyman α forest*.

In the time since the intervening cloud hypothesis was established, there have been several studies devoted to the observation and analysis of QSO Lyman α absorption lines. They have proved to be valuable probes of the high-redshift universe because:

- Some physical properties of the clouds producing them (the *Lyman α clouds*) can be deduced by fitting theoretical line profiles (see Section 1.3.1). This provides important constraints on models for the state and distribution of matter and radiation at high redshift.
- They are common enough to provide reasonable statistical samples covering large regions of space and large intervals in redshift, allowing redshift evolution and the formation of structure to be examined.
- They are observable at redshifts which span the likely epoch of galaxy formation. Therefore, studies of the Lyman α clouds may provide valuable clues to understanding the processes by which galaxies formed.

Several important findings have come from studies of the Lyman α forest, as well as several intriguing questions and problems. These will be examined after a description of the theory and methods used in analysing absorption lines, presented in Section 1.3.

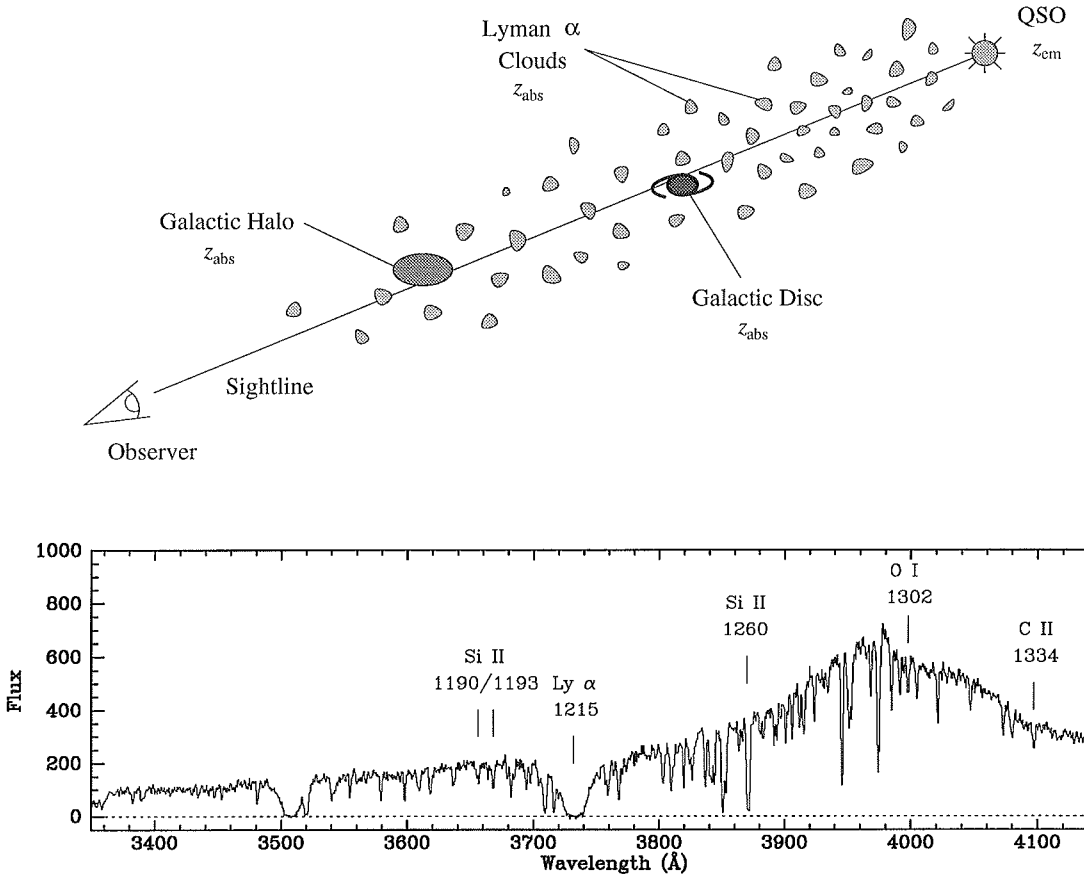

Figure 1.2 A typical QSO spectrum observed at intermediate resolution (1.5 Å FWHM), showing the absorption lines of the Lyman α forest. The sketch (not to scale) illustrates the interception of the QSO light by intervening objects at various redshifts. The QSO spectrum is for Q0049−283, from Hunstead and Pettini (private communication), with emission redshift $z_{\rm em} = 2.28$; the flux is in arbitrary units. Marked on the spectrum are a damped Lyman α line (see Section 1.3.1) at absorption redshift $z_{\rm abs} = 2.07$, and several metal lines in the same redshift system. A second damped Lyman α line is visible near 3500 Å. The absorption lines redward of the Lyman α emission peak (centred at 3990 Å, with breadth ~ 200 Å) are metal lines in various redshift systems, while most of the lines blueward are Lyman α forest lines. Damped Lyman α systems are thought to arise in galactic discs, while other metal systems arise in galactic haloes.

1.3 Studying QSO Absorption Lines

1.3.1 Voigt Profiles and the Curve-of-Growth

Given the evidence described in Section 1.2, a good working assumption is that absorption lines in QSO spectra are formed by absorption of the QSO continuum by clouds of intervening material. As the optical continuum emitting regions of QSOs are physically small ($\lesssim 0.01$ pc)[9], intervening clouds of reasonable size which are distant from the background QSO fully cover the continuum source. This configuration leads to the absorption line shape being that of a Voigt profile, which is relatively simple to model mathematically.

Voigt profiles take into account the natural line profile and Doppler broadening due to motion of the absorbing material. They are defined by five physical parameters:

1. The rest wavelength λ_0 of the atomic transition.
2. The absorption redshift $z_{\rm abs}$.
3. The transition oscillator strength f, which is a quantum mechanical constant for a given atomic transition.
4. The column density N of absorbing atoms or ions[10].
5. The velocity dispersion or Doppler parameter b of the absorbing material.

The first two parameters define the position of the line in the spectrum, the last three determine the shape of the absorption profile.

Observationally, there are two simple parameters which can be measured from an absorption line. One is the observed central wavelength $\lambda_{\rm obs}$ (after any necessary corrections for the Doppler shift caused by the Earth's motion and the refractive index of the atmosphere—these are straightforward calculations). This gives directly the value of $(1+z_{\rm abs})\lambda_0$. The particular atomic transition responsible for any given absorption line can often be identified, either by matching the inferred redshift $z_{\rm abs}$ with those inferred from other lines and deciding they arise in the same absorber, or simply by a justifiable assumption (this is explained in more detail in Section 1.3.2). Thus λ_0, f, and $z_{\rm abs}$ can be determined.

The second simple observational parameter is the observed equivalent width $W_{\rm obs}$ of a line. This is defined as

$$W_{\rm obs} = \int_{-\infty}^{+\infty} I(\lambda_{\rm obs}) d\lambda_{\rm obs}, \tag{1.1}$$

where $I(\lambda_{\rm obs})$ is the normalised, dimensionless intensity as a function of $\lambda_{\rm obs}$. More intuitively, it is the area enclosed by the normalised continuum level and the absorption profile, measured in wavelength units. For a digital spectrum, $W_{\rm obs}$ is

[9]This size is derived from light travel time arguments and the fact that QSO continuum emission has been observed to vary on timescales of less than a year. See *e.g.* Weedman (1986, pp190–193).

[10]Column densities in this thesis are always in units of cm^{-2}. Often the logarithm (to base 10) of the column density in these units is quoted: $\log(N/{\rm cm}^{-2})$, but the units are omitted for brevity.

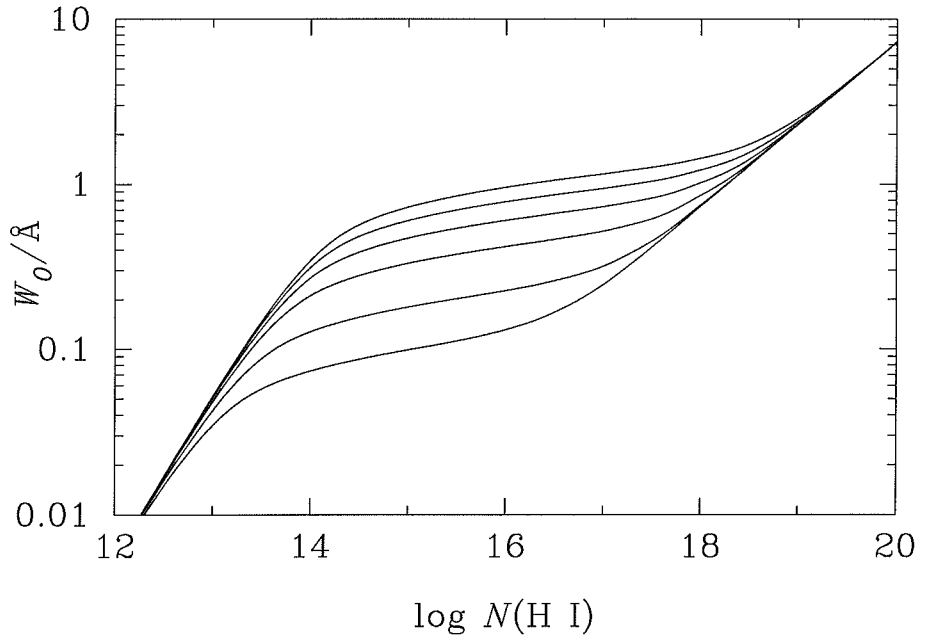

Figure 1.3 The Curve-of-Growth for Lyman α lines. The plot shows the relation between absorber column density N(H I) (measured in cm^{-2}) and rest frame equivalent width W_0, for six different values of the velocity dispersion Doppler parameter b. The curves, from bottom to top, correspond to b values of 5, 10, 20, 30, 40, and $50\,\mathrm{km\,s}^{-1}$ respectively.

calculated by summing the normalised intensities of a finite number of contiguous pixels, chosen to cover the wavelength range over which the absorption feature can be distinguished from the continuum noise, and dividing by the mean number of pixels per wavelength unit. The observed equivalent width can be converted to a rest equivalent width W_0 by the relation

$$W_{\mathrm{obs}} = (1 + z_{\mathrm{abs}})W_0. \tag{1.2}$$

The observational parameter W_{obs} depends on both b and N in a complex way (except at very low or very high N). This can be illustrated with the so-called "curve-of-growth", shown in Figure 1.3, which shows the Lyman α W_0 (Å) as a function of $\log N$(H I) for specific values of b ($\mathrm{km\,s}^{-1}$)[11].

The curve-of-growth has three regions of distinct behaviour, joined by smooth transition zones:

Linear region: The lowest column density region, extending up to $\log N(\mathrm{H\,I}) \sim 13$ for $b = 10\,\mathrm{km\,s}^{-1}$ and $\log N(\mathrm{H\,I}) \sim 14$ for $b = 50\,\mathrm{km\,s}^{-1}$. In this region the equivalent width increases directly proportionally with the column density,

$$W_0 \propto N. \tag{1.3}$$

[11]Often curves-of-growth are presented as plots of W_0/λ_0 versus $Nf\lambda_0$. This normalisation removes any dependence on the particular atomic transition, so can be used for general purposes. As this thesis is mostly concerned with the Lyman α transition of H I, the specific curves-of-growth for this transition are presented in more readily applicable units.

In the linear region, the shape of the absorption profile is sufficient to define b and N, given an arbitrarily high S/N ratio. With limited S/N, there will be fitting errors, but a useful estimate of the line parameters can usually be made. If the line shape is completely obscured by noise, or unresolved, the equivalent width can still be measured and used to obtain a value for N.

Saturated region: The central region of column density, extending over the range $14 \lesssim \log N(\mathrm{H\,I}) \lesssim 17$ for $b = 10\,\mathrm{km\,s^{-1}}$ and $15 \lesssim \log N(\mathrm{H\,I}) \lesssim 18$ for $b = 50\,\mathrm{km\,s^{-1}}$. In this region the equivalent width changes only very slowly with column density,

$$W_0 \propto \sqrt{\log N}, \tag{1.4}$$

and is much more dependent on b.

In the saturated region, the core of an absorption line effectively blocks all light and the wings are steep. With moderate S/N ratios the b value of an unblended line can usually be fitted with reasonably small uncertainty, but the value of N can easily be uncertain by an order of magnitude or more. If saturated lines are blended, however, it is very difficult to determine where one line ends and the next begins, making b values uncertain. In some cases it can be difficult even deciding if a saturated feature is a single line or several blended together.

Damped region: The region of highest column density, which extends beyond $\log N(\mathrm{H\,I}) \sim 18$ for $b = 10\,\mathrm{km\,s^{-1}}$ and $\log N(\mathrm{H\,I}) \sim 19$ for $b = 50\,\mathrm{km\,s^{-1}}$. In this region the equivalent width increases as the square root of the column density,

$$W_0 \propto \sqrt{N}, \tag{1.5}$$

and is virtually independent of b.

In the damped region, the line wings become extremely broad, but shallow. By fitting the wings, N can be determined accurately, but it is virtually impossible to determine a b value.

It is normally assumed that the absorber particles have a Maxwellian velocity distribution. The value of b is related to the standard deviation σ of the line-of-sight velocity distribution by

$$b = \sqrt{2}\,\sigma. \tag{1.6}$$

If this velocity distribution is entirely due to thermal motion, b can be related directly to the gas temperature T by

$$b^2 = \frac{2kT}{m}, \tag{1.7}$$

where k is Boltzmann's constant and m is the atomic mass. If, however, there is some bulk motion of the gas, such as turbulence, rotation, expansion, or contraction, then this motion will increase σ and hence b above the thermal value. If such bulk motion produces a velocity distribution which can reasonably be approximated by

a gaussian of standard deviation $\sigma_{\rm bulk} = b_{\rm bulk}/\sqrt{2}$, the contributions combine as follows:

$$b^2 = \frac{2kT}{m} + b_{\rm bulk}^2. \tag{1.8}$$

1.3.2 Absorption Line Identifications

Identifying the atomic species responsible for a particular absorption line is non-trivial. In addition to Lyman α absorption by intervening clouds containing H I, concentrations of other elements along the sightline can also produce absorption lines. These so-called "metal" lines have various rest wavelengths spanning a wide range both shortward and longward of Lyman α. Metal lines can therefore appear both blueward and redward of the Lyman α emission peak, unlike Lyman α absorption which appears only blueward[12]. Correctly identifying absorption lines is vital to correctly interpreting the information they contain.

Lines observed redward of the Lyman α emission peak can generally be interpreted as metal lines. Metal lines can also often be distinguished from Lyman α lines by their narrow appearance, a consequence of Equation 1.7; the higher atomic mass leads to a considerably smaller b value for gas at the same temperature. To be sure of a correct identification, though, it is necessary to identify the specific atomic transition by finding other absorption lines caused by different transitions (either in the same ionic species or a different one) at the same redshift.

Lines produced by different transitions in the same species (such as the C IV $\lambda\lambda$ 1548, 1550 doublet, the Si II $\lambda\lambda$ 1260, 1304 lines, and the Mg II $\lambda\lambda$ 2796, 2803 doublet) are particularly useful, because they are produced in gas of identical physical conditions and, if the lines are unsaturated, the ratio of their equivalent widths, or *doublet ratio*, is determined by the ratio of their oscillator strengths f. Lines which are consistent with such identifications have almost certainly been correctly identified.

Consistency of redshifts among different species is also a good indicator of correct identifications. Once a redshift for a metal line system is established, more lines can often be identified in the same system.

After an exhaustive search for metal systems, the remaining unidentified lines are usually attributed to Lyman α at various redshifts. If the spectrum extends blueward beyond the Lyman β emission wavelength, corresponding Lyman β lines can be searched for to confirm these identifications, but this is often not done for practical reasons such as wavelength coverage or instrumental sensitivity limitations.

[12]It is possible for Lyman α absorption to appear slightly redward of the emission peak, in the following two cases: (1) The Lyman α emission peak does not define the systemic redshift, but is somewhat blueward of it. This can occur because the broad line emitting region of the QSO is distinct from the continuum and narrow line emitting regions, and often has a relative velocity of $\sim 1000\,{\rm km\,s^{-1}}$ towards the observer (Gaskell, 1982; Espey *et al.*, 1989). (2) If an absorbing cloud is physically close to the QSO and has a peculiar velocity component toward it.

1.3.3 Observational Aspects of the Lyman α Forest

When a QSO spectrum is observed, there are several effects which complicate the procedure of identifying and measuring the absorption lines.

Instrumental Resolution

The instruments used to gather and record the spectrum have a non-zero wavelength resolution. The instrumental resolution profile can usually be represented adequately by a gaussian, with standard deviation $\sigma_{\rm inst} = b_{\rm inst}/\sqrt{2}$. The observed spectrum is the convolution of the true spectrum and the instrumental profile. Allowance must be made for this when fitting Voigt profiles to absorption lines.

Normalisation

The observed spectrum is not normalised. The continuum level for a QSO, in units of flux density f_ν versus wavelength λ, can be approximated reasonably over limited wavelength intervals by a power law with broad emission lines superposed. Atmospheric absorption, which increases steadily with shorter wavelengths in the ultraviolet, can then alter the observed continuum. Finally, instrumental effects such as a change in spectrograph efficiency or detector sensitivity with wavelength can change the apparent continuum shape. In particular, echelle spectrographs, which are used for high resolution absorption line studies, use diffraction gratings blazed to operate at high spectral orders and the blaze efficiency drops significantly towards the edges of each order.

Before an observed spectrum can be analysed by fitting line profiles, it must be normalised with a satisfactory continuum level. As discussed in Sections 2.2 and 3.2, this can be a highly complex procedure.

Signal-to-Noise Ratio

Observed spectra are subject to finite signal-to-noise (S/N) ratios. If a photon counting detector with negligible noise level[13] is used to collect the spectrum, photon statistics dictate the minimum noise level achievable with a given observing time. Since counting photons is a Poisson process, the standard deviation σ of the counts is

$$\sigma = \sqrt{\mathcal{N}}, \tag{1.9}$$

where $\mathcal{N}$ is the number of photon counts per bin. The S/N ratio is then $\mathcal{N}/\sigma = \sqrt{\mathcal{N}}$ per wavelength bin.

This noise level applies to a raw spectrum of an object, which includes the superimposed night sky spectrum. Before the object spectrum can be analysed the sky spectrum must be subtracted. The sky spectrum is usually obtained simultaneously

[13]Such a detector is the Image Photon Counting System (IPCS) at the Anglo-Australian Telescope, described in Section 4.2.

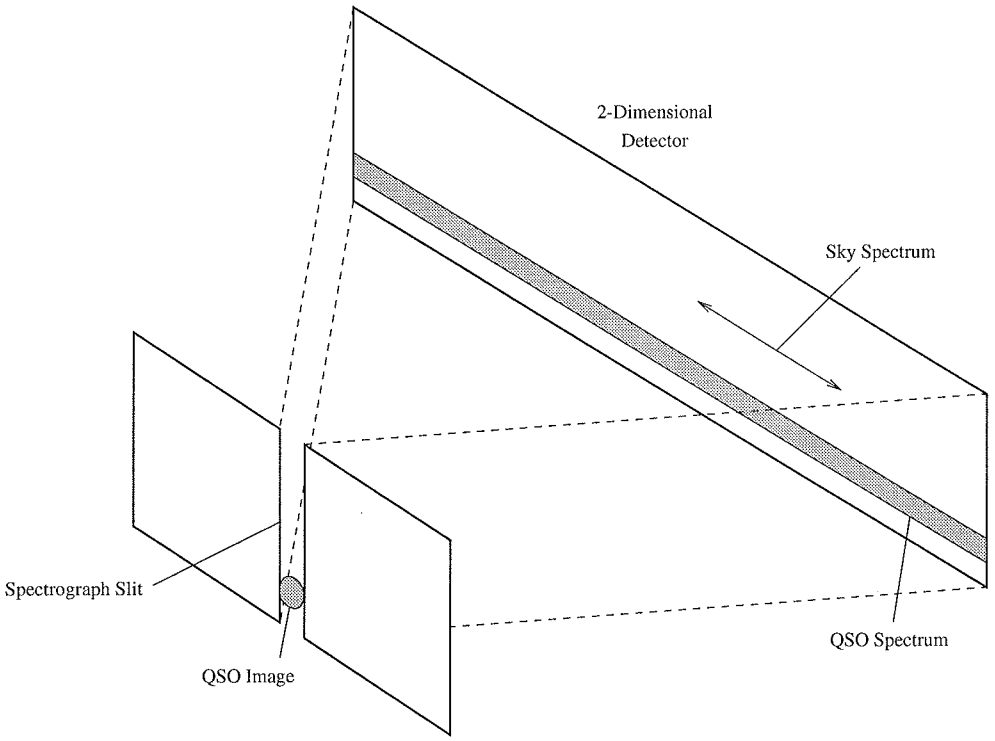

Figure 1.4 Sketch of the spectrograph slit and detector configuration for recording QSO spectra. The detector is a two-dimensional array of pixels. The spectrum is dispersed along the rows of the detector pixels by the spectrograph optics (not shown). The columns of detector pixels form an image of the spectrograph slit. The QSO spectrum is formed along a few rows of pixels, while a spectrum of the sky covers a large number of rows of pixels. In fact, the sky spectrum is also present in the same rows as the QSO spectrum, which is why a sky spectrum must be subtracted to form a spectrum of the QSO alone.

by allowing the spectrograph slit to cover a region of sky to one side of the object and recording the sky spectrum on pixels of the (2-dimensional) detector adjacent to those used for the object. This is illustrated in Figure 1.4.

If the object spectrum is extracted from $n_{\rm obj}$ rows of pixels and the sky from $n_{\rm sky}$ rows, then the resulting sky-subtracted object spectrum will have a mean noise level given by

$$\sigma^2 = \mathcal{N}_{\rm obj} + \left(\frac{n_{\rm obj} + n_{\rm sky}}{n_{\rm sky}}\right) \mathcal{N}_{\rm sky}, \tag{1.10}$$

where $\mathcal{N}_{\rm obj}$ is the mean number of photon counts per bin in the sky-subtracted object spectrum and $\mathcal{N}_{\rm sky}$ is the mean number of photon counts per bin in the sky spectrum (normalised to the same number of rows as the object spectrum). Note that in Equations 1.9 and 1.10, $\mathcal{N} = \mathcal{N}_{\rm obj} + \mathcal{N}_{\rm sky}$. The final S/N ratio $\mathcal{N}_{\rm obj}/\sigma$ is somewhat smaller than the ideal Poissonian case.

The S/N level for a faint object spectrum can be worse when detectors with appreciable noise levels, such as charge-coupled devices (CCDs) are used. CCDs

have a systematic "readout noise", which is added to all pixels during the readout of each exposure. They are also susceptible to strikes by cosmic rays. A cosmic ray hitting a CCD will produce a pixel, or small group of pixels, with an enormous signal. Such pixels must be masked out before a spectrum is generated. The number of cosmic ray strikes in a CCD frame increases in proportion to the exposure time. When detector noise is not negligible, $\mathcal{N} = \mathcal{N}_{\rm obj} + \mathcal{N}_{\rm sky} + \mathcal{N}_{\rm noise}$, and the S/N ratio of the object spectrum is degraded further. CCDs are more efficient than photon-counting devices, having quantum efficiencies $\sim$ 70–80% versus $\sim$ 10–15%, but the readout noise and cosmic rays result in lower S/N ratios for comparable observing times on very faint objects.

The presence of noise in observed spectra is unavoidable. In the present context it makes continuum fitting more difficult (see Sections 2.2 and 3.2) and can lead to significant errors in the line profile fitting procedure (Section 3.3).

Line Blending

The abundance of absorption lines in the Lyman α forest means that often line profiles will often overlap in wavelength, producing blended features. When this occurs, the profiles must be deconvolved in order to produce correct fit parameters. The deconvolution is not straightforward, especially when the S/N ratio is low, and there are generally an arbitrary number of different possibilities for assigning components to a complex blend. It is inevitable that in some cases the wrong number of components will be fitted, resulting in systematic errors in the fitted parameters.

The problems associated with line blending are discussed in several different contexts in Sections 2.1.1, 2.1.2, 2.3.2, 6.2.2, 6.3, 6.3.2, and 7.1.1.

1.4 QSO Absorption Studies

1.4.1 The Gunn-Peterson Effect

One of the implications of finding discrete absorption lines blueward of the Lyman α emission peak in QSOs was noted by Gunn and Peterson (1965) after the first spectroscopic observation of Lyman α emission, in the QSO 3C 9 (Schmidt, 1965).

Gunn and Peterson pointed out that distributed neutral hydrogen in the intergalactic medium (IGM) along the sightline to the QSO would absorb Lyman α photons at all redshifts from zero to the QSO $z_{\rm em}$, and that the resulting depression of the continuum relative to that redward of Lyman α emission provides an extremely sensitive test for such material. Measurements on Schmidt's spectrum of 3C 9 provided an immediate upper limit to the number density of H I at $z \sim 2$ of $n(\mathrm{H\,I}) = 6 \times 10^{-11} h\,\mathrm{cm}^{-3}$ for a cosmological deceleration parameter[14] of $q_0 = \frac{1}{2}$

[14]The cosmological deceleration parameter q_0 is a dimensionless measure of the deceleration of the universal Hubble expansion. $q_0 = \frac{1}{2}$ corresponds to an open, Euclidean universe, $q_0 < \frac{1}{2}$ corresponds to an open universe with negative curvature, $q_0 > \frac{1}{2}$ corresponds to a closed universe

and Hubble parameter[15] $H_0 = 100h\,\mathrm{km\,s^{-1}\,Mpc^{-1}}$. This measurement was some five orders of magnitude below the contemporary limit at $z = 0$ from 21 cm radio observations.

This exceedingly small density of H I implied either that the amount of hydrogen in the IGM was six orders of magnitude lower than any reasonable cosmological theory predicted, or that the IGM was almost completely ionised. Collisional ionisation was shown to be inadequate, so a photoionising flux of sufficient strength was indicated.

Steidel and Sargent (1987) showed that the H I density scaled as $(1 + z)^3$ for $z \lesssim 4$, and provided a new limit of $n(\mathrm{H\,I}) < 2.0 \times 10^{-11} h\,\mathrm{cm^{-3}}$ at $z = 2.64$ for $q_0 = \frac{1}{2}$. Their study of 8 QSOs produced a value for the Gunn-Peterson optical depth of $\tau_{\mathrm{GP}} < 0.06 \pm 0.06$, consistent with 0 and corresponding to a $n(\mathrm{H\,I})$ limit 6 times smaller than Gunn and Peterson's[16].

Jenkins and Ostriker (1991) showed that a measurement of the mean normalised continuum level depression between the Lyman α and Lyman β emission lines D_{A} could be used to search for Gunn-Peterson absorption. They compared the measured value of D_{A} in a sample of QSOs collected from the literature with those produced in simulations. They concluded that at $z_{\mathrm{abs}} \sim 3$ there is $\sim 30\%$ more Lyman α opacity than can be attributed to measurable lines. This excess absorption could have been due to lines of small column density or continuous absorption. Jenkins and Ostriker also showed that an examination of the distribution of residual pixel intensities in high resolution spectra of the Lyman α forest region should provide a more sensitive test for the existence of Gunn-Peterson absorption.

More recently, Giallongo *et al.* (1992) measured a value of $\tau_{\mathrm{GP}} = 0.013 \pm 0.026$ at $z = 3$, and Giallongo *et al.* (1994) measured $\tau_{\mathrm{GP}} = 0.02 \pm 0.03$ at $z = 4.3$. Using reasonable models of the thermal history of the IGM from Miralda-Escudé and Rees (1993), Giallongo *et al.* (1994) calculated an upper limit to the baryon density of the IGM of $\Omega_{\mathrm{IGM}} \sim 0.01$, in units of the critical density[17]. This value is difficult to reconcile with baryon density estimates from standard hot Big Bang nucleosynthesis models (Walker *et al.*, 1991) and luminous matter observations. It implies either that a significant number of baryons are in bound, non-luminous systems—such as Lyman α clouds—by $z \sim 5$, or that the intergalactic medium is essentially fully ionised at $z \leq 5$.

---

with positive curvature. The true value of q_0 is unknown.

[15]The value of the Hubble parameter is not known precisely, but is generally believed to lie within the range 50–$100\,\mathrm{km\,s^{-1}\,Mpc^{-1}}$. The value of h is therefore most probably in the range 0.5–1.0.

[16]Jenkins and Ostriker (1991) pointed out an error in Steidel and Sargent's paper which caused them to underestimate their optical depth measurement at $\tau_{\mathrm{GP}} < 0.02 \pm 0.03$, and led them to state an incorrect limit of $n(\mathrm{H\,I}) < 8.4 \times 10^{-12} h\,\mathrm{cm^{-3}}$ at $z = 2.64$ for $q_0 = \frac{1}{2}$. The limits shown in the main text are the corrected ones.

[17]The critical density of the universe Ω_{crit} is the average mass density required to make the universe Euclidean ($q_0 = \frac{1}{2}$).

1.4.2 The Equivalent Width Distribution

For several years, all observations of QSO absorption lines were made at intermediate to low resolution ($\sim$ 1–10 Å). At these resolutions the vast majority of the absorption lines are unresolved. Lines at close wavelength spacings will also be blended together through convolution with the instrumental resolution profile. Such unresolved and blended lines can still be used to analyse statistically the total line population and its wavelength and equivalent width distributions. Little else can be achieved, however, and even such simple measures of the line population are prone to error when line blending is significant (Parnell and Carswell, 1988).

Nevertheless, SYBT published an extensive study of the Lyman α lines in a sample of six QSO spectra in 1980. They fitted an exponential form to the observed equivalent width distribution, given by

$$\frac{\partial^2 \mathcal{N}}{\partial z \partial W} = \frac{\mathcal{N}^*}{W^*} \exp(-W/W^*)\,(1+z)^\gamma, \tag{1.11}$$

where $\partial^2\mathcal{N}/\partial z\partial W$ is the partial differential number density of clouds with respect to z and W, and $\mathcal{N}^*$ and W^* are empirical parameters (which may vary with z). SYBT fitted values of $\mathcal{N}^* = 154 \pm 11$ and $W^* = (0.36 \pm 0.02)$ Å to the lines in their data with $W_0 \geq 0.32$ Å. The cutoff was imposed at low equivalent widths because the samples were incomplete at low line strengths—weak lines are difficult to detect in noisy data.

SYBT's paper was a watershed in the study of the Lyman α forest. They were the first to analyse rigorously a large sample of Lyman α lines, establishing the intervening, cosmologically distributed cloud model for the absorbers and showing the potential of such studies for measuring physical conditions in absorbing clouds and the IGM at high redshifts.

1.5 Distributions and Evolution of the Lyman α Clouds

The full potential of QSO absorption spectra for supplying useful information about the early universe began to be realised when Carswell *et al.* (1984) observed the $z_{\rm em} = 2.147$ QSO 1101−264[18] (Osmer and Smith, 1977) at a spectral resolution of 0.25 Å. With this resolution, enough lines were resolved to allow fitting of Voigt profiles and study of the physical parameters b and N.

[18]Several authors have later referred to this object as Q1100−264, notably Carswell *et al.* (1991). The reasoning is that the object's coordinates have been revised from $11^{\rm h}01^{\rm m}00\overset{\rm s}{.}0$, $-26°28'40\overset{''}{.}0$ (Burbidge *et al.*, 1977) to $11^{\rm h}00^{\rm m}59\overset{\rm s}{.}9$, $-26°29'04\overset{''}{.}9$ (Hewitt and Burbidge, 1993) (B1950). However, standard International Astronomical Union (IAU) practice is not to change alphanumeric names once bestowed, unless incorporating more digits of information (Working Group on Designations from Commission 5 of the IAU, 1991). Since this has not been done, the original name Q1101−264 has been retained.

1.5.1 The Column Density Distribution

Using their Lyman α data for Q1101−264, Carswell *et al.* (1984) fitted a power law distribution of the form

$$\frac{d\mathcal{N}}{dN} = A_0 N^{-\beta}, \tag{1.12}$$

for values of neutral hydrogen column density $N(\mathrm{H\,I}) > 10^{13}\,\mathrm{cm}^{-2}$, with $\beta = 1.68 \pm 0.10$. They rightly pointed out that such a power law must become invalid at low column densities in order for the total number of clouds $\int_0^\infty d\mathcal{N}$ to be finite. They concluded that such a cut-off occurred below their detection limit, although above $N = 10^{12}\,\mathrm{cm}^{-2}$ because of a lack of any sign of a significant population of weak lines in their spectrum.

Subsequent research on the Lyman α cloud column density distribution and the implications of the various measurements, are presented in detail in Section 6.2.

1.5.2 The Velocity Dispersion Distribution

By measuring the velocity dispersions of a sample of Lyman α lines, Carswell *et al.* (1984) were able to examine the predictions of various theoretical models. The models gave expected ranges for the temperatures of the Lyman α clouds and, by Equation 1.8, the velocity dispersions give upper limits on the temperatures. By comparing these values, Carswell *et al.* concluded that the model of Black (1981), which predicted higher temperatures than competing models, was unlikely to be correct. (Further details of cloud models are discussed in Section 1.6.)

Carswell *et al.* also found a few lines with b values too low to be explained by any of the available models. They concluded that either the lines were unidentified metal lines, or that noise in the spectrum had produced spurious fit parameters. Further work on the Lyman α cloud velocity dispersion distribution and its interaction with various proposed cloud models is presented in detail in Section 6.4.

1.5.3 The Redshift Distribution

The determination of the number density distribution of Lyman α clouds with redshift initially had a controversial history. If the clouds were of unevolving cross section and constant comoving space density, the differential number density would vary as

$$\frac{d\mathcal{N}}{dz} \propto (1+z)(1+2q_0 z)^{-1/2}. \tag{1.13}$$

For $q_0 = \frac{1}{2}$ or 0 this corresponds to the power law distribution

$$\frac{d\mathcal{N}}{dz} \propto (1+z)^{\gamma}, \tag{1.14}$$

with $\gamma = 0.5$ or 1, respectively. In practice, only clouds producing absorption features above some S/N-dependent equivalent width limit can be used to deduce a value for γ.

SYBT were the first to examine the redshift distribution with a homogeneous sample. Fitting the data above their equivalent width completeness limit of $W_0 \geq 320\,\mathrm{m\AA}$ from their five QSO sample to Equation 1.14, they found $\gamma = 0.48 \pm 0.54$, consistent with no evolution (for $0 \leq q_0 \leq \frac{1}{2}$). Later studies found evidence for evolution, but with both $\gamma > 1$ (Young *et al.*, 1982; Carswell *et al.*, 1982) and $\gamma < 0$ (Carswell *et al.*, 1982; Phillips and Ellis, 1983).

Murdoch *et al.* (1986) presented a critical reappraisal of the previous work and established firm evidence for evolution, with a value of $\gamma = 2.17 \pm 0.36$ obtained by maximum likelihood estimates[19]

Since the redshift evolution of the Lyman α clouds was established, there have been several other interesting developments, described in detail in Section 6.3.

1.5.4 The Proximity Effect and the Ionising Background Flux

In their comprehensive analysis of the Lyman α cloud redshift distribution, Murdoch *et al.* (1986) also presented evidence for a significant countervailing trend in the spectra of individual QSOs, with the number of Lyman α lines present near the Lyman α emission peak being fewer than expected from the global distribution. This so-called "inverse effect" explained the disparate results of previous researchers and raised the possibility that hydrogen clouds within $\sim 4\,\mathrm{Mpc}$ of luminous QSOs suffered enhanced ionisation from them[20]. Murdoch *et al.* recalculated their value for the Lyman α cloud evolutionary parameter excluding regions where the Lyman α emission peak was judged to be above the continuum, obtaining $\gamma = 2.31 \pm 0.40$ and concluding that their value of $\gamma = 2.17 \pm 0.36$ was likely a lower limit.

The inverse effect was seized upon by Bajtlik *et al.* (1988), who provided evidence for the enhanced ionisation explanation and observed that, by fitting a quantitative physical model, one could infer the intensity of the background H ionising flux ($h\nu > 13.6\,\mathrm{eV}$) at high z. Their analysis produced a value for the Lyman limit intensity of

$$J_\nu = 10^{-21.0\pm0.5}\,\mathrm{erg\,cm^{-2}\,s^{-1}\,Hz^{-1}\,sr^{-1}}, \tag{1.15}$$

which was constant for $1.7 < z < 3.8$. Since this was appreciably greater than the integrated Lyman limit flux of observed QSOs at $z > 3$, it implied another source of ionising photons at high z—either dust-obscured (hence unobserved) QSOs or a more exotic source. The reality of this effect meant that the estimate of the cloud number density evolution index γ made by Murdoch *et al.* (1986) was too low. Bajtlik *et al.* calculated that the region of space surrounding a QSO which would be affected by the enhanced ionising flux would have a radius of $\sim 5h^{-1}\,\mathrm{Mpc}$.

[19]SYBT also used the method of maximum likelihood to determine a value for γ, but they applied it incorrectly.

[20]Murdoch *et al.* also postulated an alternative explanation: That the Lyman α clouds were sufficiently small that they did not fully occult the QSO broad emission line region when they were close to the QSO. This explanation has since been abandoned.

By removing lines within this region of space around each QSO from the sample of Murdoch *et al.*, they produced a corrected value of $\gamma = 2.36 \pm 0.40$. Bajtlik *et al.* also renamed the inverse effect as the "proximity effect", because of their evidence for its origin.

The "proximity effect" explanation was briefly argued against by Crotts (1989). By examining the Lyman α forests of a tight grouping of four QSOs on the sky, Crotts found no evidence for enhanced ionisation in the vicinity of the foreground QSOs, and proposed that isotropic radiation from QSOs was inadequate to explain the effect.

Lu *et al.* (1991) performed an exhaustive analysis of 950 Lyman α lines with $1.7 < z_{\rm abs} < 3.8$ and $W_0 > 0.36$ Å from the spectra of 38 QSOs, finding strong evidence for the reality of the proximity effect. They also calculated an improved distance within which the ionising flux from a QSO would be expected to significantly affect the properties of the Lyman α forest clouds. This distance was $8h^{-1}$ Mpc, somewhat greater than the distances used by Murdoch *et al.* and Bajtlik *et al.*.

Dobrzycki and Bechtold (1991) found a highly significant void of Lyman α absorption lines in the spectrum of the $z_{\rm em} = 3.29$ QSO 0302−003 near the redshift of a nearby foreground QSO. The redshifts of the void and the foreground QSO were slightly different, which Dobrzycki and Bechtold used to argue that the ionising radiation from the QSO was not isotropic.

Noting the dearth of Lyman α forest lines with $\log N({\rm H\,I}) > 15$ in published data, Meiksin and Madau (1993) proposed that the opacity of the universe at high redshift may be 1.5–3 times lower than previous estimates. This led to a new estimate for the contribution of integrated QSO flux of $J_\nu \sim 3 \times 10^{-22}\,{\rm erg\,cm^{-2}\,s^{-1}\,Hz^{-1}\,sr^{-1}}$ at $z = 3$–5, for $q_0 = \frac{1}{2}$. This was closer to the total metagalactic ionising flux estimated by Bajtlik *et al.* (1988), but still inconsistent.

In a sample of 34 QSOs observed at intermediate spectral resolution, Bechtold (1994) found strong evidence for the reality of the proximity effect. The data implied a metagalactic ionising flux of $J_\nu \sim 3\times10^{-21}\,{\rm erg\,cm^{-2}\,s^{-1}\,Hz^{-1}\,sr^{-1}}$ for $1.6 < z < 4.1$, at the high end of the range derived by Bajtlik *et al.* (1988), and further removed from the estimates of the integrated QSO contribution.

Cristiani *et al.* (1995) used the proximity effect in their study of the $z_{\rm em} = 3.66$ QSO 0055−269, combined with data on Q2206−199N ($z_{\rm em} = 2.56$) (Pettini *et al.*, 1990) and three other QSOs (Giallongo *et al.*, 1993), to establish a value of $J_\nu = 5 \times 10^{-22}\,{\rm erg\,cm^{-2}\,s^{-1}\,Hz^{-1}\,sr^{-1}}$ for the UV background flux at $1.8 \lesssim z \lesssim 3.66$. Taking into account uncertainties in the QSO luminosity function, Cristiani *et al.* considered this to be consistent with the contribution from QSOs of $J_\nu = 3 \times 10^{-22}\,{\rm erg\,cm^{-2}\,s^{-1}\,Hz^{-1}\,sr^{-1}}$ derived by Meiksin and Madau (1993), though they did not dismiss the possibility of other UV background sources accounting for the difference in the best values.

As can be seen from the results mentioned, it is not yet clear whether the metagalactic ionising flux at high redshift, as measured by the proximity effect, is consistent with the estimated global contribution from QSOs. Future work involving large samples of Lyman α lines observed at high resolution may allow the measurement

to be constrained adequately.

1.6 Physical Models of Lyman α Clouds

In their landmark paper, SYBT were the first to propose a physical model for Lyman α clouds. Using their intermediate-resolution data, SYBT determined that the clouds were large, tenuous, and hot, with typical diameters $d \sim 10\,\mathrm{kpc}$, hydrogen number densities $n(\mathrm{H}) \sim 10^{-4}\,\mathrm{cm}^{-3}$, and temperatures $T \sim 3 \times 10^4\,\mathrm{K}$. Some form of confinement was necessary because the sound speed in such hot gas is high enough that a freely expanding cloud of size 10 kpc would dissipate in much less than a Hubble time. SYBT showed that the cloud masses (estimated to be $\sim 10^5\,\mathrm{M}_\odot$) were insufficient to confine them gravitationally, so they adopted the pressure-confined model.

In SYBT's model, the clouds were photoionised by the integrated background ultraviolet flux from QSOs, and the resulting ionisation level was high, with neutral fraction $n(\mathrm{H\,I})/n(\mathrm{H}) \sim 10^{-4}$. The confining IGM was necessarily hotter and more tenuous than the clouds. Since the properties of the IGM at high redshift are relatively unconstrained, its pressure and density could be adjusted freely to fit the model.

The simple model of SYBT was elaborated by Ikeuchi and Ostriker (1986), Ostriker *et al.* (1988), and Baron *et al.* (1989). Baron *et al.* showed that confinement by a constant IGM pressure was insufficient to account for the large observed range of H I column densities. They proposed that high $N(\mathrm{H\,I})$ clouds may exist within regions of higher-than-average gas density which are themselves gravitationally confined.

Several other models for the Lyman α clouds have been proposed, including:

- Clouds which are gravitationally confined by "minihaloes" of dark matter. Rees (1986) showed that a standard cold dark matter (CDM) cosmology with initial density fluctuation spectrum sufficient to produce the observed number of galaxies would inevitably also produce dark minihaloes. These minihaloes would collect and confine hydrogen with neutral column densities similar to those seen for Lyman α clouds.
- A mixture of freely expanding and gravitationally collapsing clouds, forming the low-mass end of primordial density fluctuations in a CDM universe (Bond *et al.*, 1988). This model requires the Lyman α clouds to vanish rapidly and completely at $z \lesssim 2$, which has been shown not to occur by HST observations of 3C 273 (Morris *et al.*, 1991).
- Thin "pancakes" of hydrogen, formed by shocks in thermally unstable clouds of gas (Hogan, 1987). Such sheets of gas would be at higher pressure than the clouds in the models mentioned above, and have much higher densities and neutral fractions and lower temperatures.

For all but the last model, the temperature of the Lyman α clouds is set at $T \sim 3 \times 10^4\,\mathrm{K}$ by photoionisation. This corresponds to a minimum velocity dispersion of $b \sim 22\,\mathrm{km\,s^{-1}}$, by Equation 1.8. Any strong evidence for the existence of Lyman α lines with $b < 20\,\mathrm{km\,s^{-1}}$ would therefore pose severe difficulties for the simple pressure-confined and minihalo models. Such evidence has accumulated over recent years, and it is discussed in detail in Section 6.4, together with the ramifications for theoretical models of the Lyman α clouds.

1.6.1 QSO Pairs and Gravitationally Lensed QSOs

In addition to supplying predictions of Lyman α cloud temperatures, theoretical models can predict a range of cloud dimensions. These come about through the application of an ionisation model, which defines the hydrogen ionisation level and number density. Under the assumption that the clouds are approximately spherical (which *may* not be the case in reality), dividing a typical observed neutral hydrogen column density by the predicted neutral hydrogen number density gives the expected linear dimension of a cloud.

One method of directly measuring the sizes of Lyman α clouds is to examine the sightlines of close QSO pairs or gravitationally lensed QSO images. If absorption is seen at a common z_{abs} in two sightlines, it implies the intervening cloud has a transverse dimension at least as large as the separation between the sightlines at that redshift—or that smaller clouds form coherent groupings on similar scales.

An upper limit of $d \sim 1$–$2\,\mathrm{Mpc}$ was set on the cloud sizes by Sargent *et al.* (1982), who found no correlation between the redshifts of Lyman α lines in the spectra of two QSOs separated by $3'$.

Weymann and Foltz (1983) were the first to make a detection of correlated absorption, finding two common Lyman α lines in the spectra of two images of the triply-lensed, $z_{\mathrm{em}} = 1.72$ QSO PG 1115+08, separated by $2''.3$. Unfortunately, the redshift of the lensing object was unknown, but assuming it was $z_{\mathrm{lens}} = 0.8$–1.0 led to a minimum cloud diameter estimate of $\sim 250h^{-1} < d < 300h^{-1}\,\mathrm{pc}$ for $q_0 = \frac{1}{2}$ and spherical clouds.

Foltz *et al.* (1984) found some common Lyman α lines, as well as some lines not present in both images, in the spectra of the $z_{\mathrm{em}} = 2.19$ QSO pair 2345+007A, B[21]. They concluded that a typical size for Lyman α clouds was $2h^{-1} < d < 10h^{-1}\,\mathrm{kpc}$ for $q_0 = \frac{1}{2}$ at $z \sim 2$.

[21]The lensed nature of this QSO pair has not been established beyond doubt. The image separation of $7''.1$ is the largest proposed for a lensed QSO, and no lensing object has yet been seen. Steidel and Sargent (1990) found differences between the emission line to continuum ratios for the images and concluded the images were two different objects. Steidel and Sargent (1991), using better quality data, found the detailed emission line profile shapes to be so similar that they concluded the images *were* a lensed pair, and that the differences found by Steidel and Sargent must be caused by either microlensing of different regions within the QSO environment or by temporal variations coupled with the light delay time between the two images. Fischer *et al.* (1994) and McLeod *et al.* (1994) describe recent, fruitless attempts to image the lensing object, which must have mass $\sim 10^{13}\,\mathrm{M}_\odot$ if the images are indeed lensed.

In a study of the $z_{\rm em} = 2.73$ gravitationally lensed QSO pair UM 673A, B (angular separation $\Delta\theta = 2\farcs22$), Smette *et al.* (1992) found a large number of coincident Lyman α lines in the two images. They estimated a 2σ confidence limit range of $5h^{-1} < d < 60h^{-1}$ kpc ($q_0 = \frac{1}{2}$) for the diameters of spherical Lyman α clouds at $z \sim 2.5$. Smette *et al.* addressed the concern that correlated absorption may occur if the sightlines cross clusters of small clouds, with clustering scales of the order of the size estimates, rather than individual clouds of such size. They showed a strong correlation with unity slope (but substantial scatter) between the equivalent widths of the Lyman α lines at corresponding redshifts in the two sightlines, which they regarded as strong evidence that the sightlines actually crossed the same clouds. However, the correlation in W_0 was based mostly on lines with $0.25 < W_0 < 1.0$ Å, where the Lyman α lines are on the saturated part of the curve-of-growth. This means that large variations in the column densities of the absorbers between the sightlines would translate to small differences in W_0, so the correlation between N(H I) values cannot be explored adequately.

In separate studies of the same QSO pair 1343+266A, B[22] ($z_{\rm em} = 2.029$, 2.031, $\Delta\theta = 9\farcs5$), Bechtold *et al.* (1994) and Dinshaw *et al.* (1994) used Lyman α line coincidences between the sightlines to conclude that the cloud sizes were $40h^{-1} < d < 300h^{-1}$ kpc at $z \sim 1.8$, with a most probable diameter $d = 70h^{-1}$ kpc. Dinshaw *et al.* noted that the corresponding absorption lines in the two spectra did not have equivalent widths correlated with unit slope, and on average were significantly offset in velocity from each other. They deduced that there were significant differences in the physical properties of the clouds on scales of tens of kiloparsecs. The velocity offsets, although significant, were $\sim 60\,{\rm km\,s^{-1}}$, which is smaller than the expected value of 200–300 $\rm km\,s^{-1}$ for discrete clouds in the disc or virialised halo of a galaxy. This provided a constraint on models in which the clouds were small, but clustered on scales of $\sim 100h^{-1}$ kpc. Both groups pointed out that the implied cloud sizes were larger than predicted by any reasonable model. Bechtold postulated that the Lyman α clouds at $z \sim 2$ may be the collapsing progenitors of faint blue galaxies.

Smette *et al.* (1995) observed the QSO pair HE 1104−1805A, B ($z_{\rm em} = 2.31$, $\Delta\theta = 3\farcs0$)[23] and found 95 common Lyman α lines in the spectra. They derived a lower limit cloud diameter of $d > 50h^{-1}$ kpc at $z \sim 2$. They also found that the equivalent widths of corresponding lines were strongly correlated, which was incompatible with the popular spherical mini-halo model of Lyman α clouds (Meiksin, 1994). Smette *et al.* proposed that the Lyman α clouds were more likely to be flattened structures, such as discs or "pancakes".

The results from QSO pair studies reveal details of the transverse sizes of the Lyman α clouds. If the clouds are flattened structures, then other information must be used to derive the dimensions along the line of sight. Some measurements of this dimension, and the consequences in the context of the transverse measurements, are

[22]Dinshaw *et al.* (1994) refer to these objects as Q1343+2640A, B.

[23]The two QSO images have similar redshifts, but it has not yet been determined if they are gravitationally lensed images or separate objects.

discussed in detail in Section 6.4.

1.6.2 Lyman α Cloud-Galaxy Associations

Recently, Lanzetta *et al.* (1995) examined fields around six *Hubble Space Telescope* spectroscopic target QSOs, obtaining images and spectra of 46 galaxies spanning $0.07 < z < 0.55$. By finding galaxies coincident in redshift with Lyman α lines in the QSO spectra (to within $\Delta v = 250\,\mathrm{km\,s^{-1}}$), they showed that a large fraction (at least 0.35 ± 0.10) of such lines at $z_{\mathrm{abs}} \lesssim 1$ may arise in the outer haloes of luminous galaxies. An anti-correlation of the Lyman α equivalent width with the impact parameters of the galaxies to the QSO sightlines strengthened the claim and provided a measure of the typical size of the Lyman α envelopes of $\sim 160h^{-1}$ Mpc.

The results of Lanzetta *et al.* directly contradict the original assertion of SYBT that the Lyman α clouds form a cosmological population of objects unassociated with luminous galaxies. The evolution of opinions on the nature of the Lyman α cloud population is discussed in detail, in the context of the work presented in this thesis, in Section 6.5.

1.7 Large-Scale Clustering

Studies of the distribution of galaxies and galaxy clusters indicate that the local universe is inhomogeneous on scales of up to $\sim 100h^{-1}$ Mpc (Bahcall, 1988, and references therein). Theoretical models have yet to explain adequately how such large structures came about, and several *ad hoc* theories have been proposed. It is not even clear whether large structures formed first, then fragmented into the clusters and galaxies we see today (the "top-down" scenario), or the galaxies formed first and then collected into aggregates that became clusters and superclusters (the "bottom-up" scenario).

In order to draw a consistent picture of the formation and evolution of galaxies and other structures in the universe, observational evidence from many sources and theoretical models must be combined. Of particular importance are observations which reveal information about the evolution of structure at high redshifts, because these can provide strong constraints on the timescales over which structure-formation models must operate.

1.7.1 Lyman α Clouds as Probes of Clustering

The clouds of the Lyman α forest provide an excellent probe for the investigation of large-scale clustering in the early universe. They are numerous at $z \gtrsim 2$ and data from a large sample of them can be collected with the observation of a single QSO. The clouds span a large range in redshift, being detectable all the way from $z \sim 0$ with the *Hubble Space Telescope* up to $z \sim 4.9$ along the sightlines to the highest redshift QSOs known.

Statistical analyses of the redshift distribution of Lyman α clouds can reveal structures on scales from $\sim$ 1–100 Mpc or more. Details of studies of clustering in the Lyman α forest and the implications of the work to date are presented in Chapter 7.

1.8 Outline of Thesis

The remainder of this thesis is organised as follows:

Chapter 2: Describes the "Cloudy Night QSO", a detailed simulation of a QSO spectrum upon which the data reduction and analysis techniques used in this thesis were tested. The results of those analyses are presented.

Chapter 3: Describes the input data which comprised the Cloudy Night QSO spectrum and presents measurements and analyses of the errors introduced in the data reduction.

Chapter 4: Describes the QSOs observed and the data reduction techniques applied to the spectra.

Chapter 5: Details the heavy element absorption systems in the observed QSO spectra.

Chapter 6: Presents studies of the measured parameters of the Lyman α lines in the QSO spectra and discusses the implications of the results.

Chapter 7: Presents an examination of the clustering properties of the Lyman α clouds.

Chapter 8: Describes work on some incidental topics which arose from the analyses of the data. These include a study of possible structure in the Lyman α emission lines of the QSOs, a discussion of the differences between QSO sightlines, and a search for metals in the Lyman α forest systems.

Chapter 9: Summarises the main results of the thesis and presents suggestions for future work.